Applied Catalysis B: Environmental 140–141 (2013) 1–8

Contents lists available at SciVerse ScienceDirect

Applied Catalysis B: Environmental

journal homepage: www.elsevier.com/locate/apcatb

Enhancing the performance of Co_3O_4/CNTs for the catalytic combustion of toluene by tuning the surface structures of CNTs

Shujuan Jiang, Shaoqing Song*

Key Laboratory of Radioactive Geology and Exploration Technology Fundamental Science for National Defense, School of Chemistry, Biology and Material, East China Institute of Technology, Nanchang, Jiangxi Province 330013, PR China

ARTICLE INFO

Article history:
Received 23 January 2013
Received in revised form 17 March 2013
Accepted 26 March 2013
Available online 1 April 2013

Keywords:
Catalytic combustion
VOCs
Co_3O_4/CNTs
Defects
—COOH groups

ABSTRACT

The catalytic performance of the supported Co_3O_4 on CNTs (Co_3O_4/CNTs) in the catalytic combustion of toluene was improved by tuning the surface structures of CNTs. The study results showed that the surface defect structures of CNTs could not only enhance the ability of Co_3O_4 to develop reduction/oxidation cycles, but also increase the proportion of the adsorbed oxygen species to the surface lattice oxygen ones. Thus, the defects of CNTs could improve the catalytic activity of Co_3O_4/CNTs and lower the complete conversion temperature of toluene. Moreover, the CO_2 selectivity increased along with increasing the —COOH amount of the CNTs. Therefore, by tuning the defect density and —COOH amount, the conversion of toluene was completed at 257 °C and the selectivity to CO_2 achieved to ~100% on Co_3O_4/CNTs-120 catalyst, which is much better than Co_3O_4/Beta, Co_3O_4/ZSM-5 or Co_3O_4/SBA-15. Furthermore, compared with Pd/Beta and Pd/SBA-15 catalysts, Co_3O_4/CNTs showed a similar or even better catalytic performance, indicating the great potential application of Co_3O_4/CNT catalysts for the catalytic combustion of toluene.

1. Introduction

The catalytic combustion of volatile organic compounds (VOCs) to control gaseous industrial emissions is one of the most promising environmental technologies [1,2], and they most commonly use Pd or Pt as the catalysts [2–13]. However, their wide industrial applications are hindered by the very limited reserves and high cost. Hence, there are strong interests to develop alternative efficient metal oxide catalysts for VOC oxidation, especially utilizing natural abundant cheap resources. Therefore, transition metal oxides were often chosen as promising catalysts for VOC combustion to rival Pd or Pt in activity and durability [14–25]. Study results show that the catalytic activity and selectivity of the transition metal oxide catalysts are mainly related to their crystallite size and morphology [26,27]. However, from the view point of the practical application, the synthesis of the catalysts often requires tedious and complicated operations. Thus, how to facilely improve the catalytic performance of transition metal oxide catalysts in the catalytic combustion of VOCs would be the main challenge to be resolved. Here, we aimed to regulate the surface structure of supports to tune the electronic structure of transition metal oxides catalysts. However, traditional supports, such as SiO_2, γ-Al_2O_3, silica-alumina, and various zeolites, present low thermal conductivity and high hydrophilicity, which means that the water generated by the combustion reactions can be chemisorbed, so blocking the active sites of the catalysts.

Carbon nanotubes (CNTs) are considered as one of the promising supports due to the good electrical conductivity, mechanical strength, and thermal stability [28]. The surface structures of CNTs are composed of graphitize, oxygen-containing groups (—COOH) and defects [29]. And these surface structures show the unique chemical and physical properties. For example, Yang et al. reported the surface —COOH of CNTs exhibited high activity in the wet air oxidation of phenol [30]. We have previously confirmed that the defects of CNTs could activate CuO nanoparticles (NPs) and enhance the selectivity to N_2 in the catalytic oxidation of NH_3 [31]. In this paper, Co_3O_4 NPs as typical transition metal oxide catalysts were deposited on the surface of CNTs for the catalytic combustion of toluene. We intended to study the effects of the surface structures of CNTs on the catalytic performance of Co_3O_4 and ultimately the feasibility of tuning the catalytic performance by facilely regulating the useful surface structures of CNTs. The study results showed that the surface defects could lower the reaction temperature, and the —COOH on CNTs enhance the selectivity to CO_2. Thus, the catalytic performance of Co_3O_4 on CNTs was improved with increasing the defect and —COOH density. Consequently, Co_3O_4 on CNTs showed similar or even superior catalytic performance to Pd/Beta or Pd/SBA-15 catalysts.

* Corresponding author. Tel.: +86 791 83896550; fax: +86 791 83896550.
E-mail address: sqsong@ecit.edu.cn (S. Song).

0926-3373/$ – see front matter © 2013 Elsevier B.V. All rights reserved.
http://dx.doi.org/10.1016/j.apcatb.2013.03.040

2. Experimental details

2.1. Preparation of the catalysts

1 g of CNTs (Chengdu Organic Chemicals) were suspended in 50 ml of concentrated HNO_3 (68 wt.%) and followed by ultrasonic process at room temperature for 60, 80, 100, 120 and 140 min, respectively, and then filtrated. These filtrated CNTs were all washed thoroughly with deionized water until the pH was around 7, and then dried at 60 °C for 12 h. 0.5 g of the treated CNTs were impregnated into 20 ml of $Co(CH_2COO)_2$ aqueous solution under stirring followed by ultrasonic treatment for 25 min. Then the solvent was evaporated slowly under ambient conditions. The resulting solid mixture was gradually heated to 120 °C in air and kept for 3 h before being heated to 400 °C at a rate of 2 °C/min in He and held there for 3 h. The prepared nanocomposites were denoted as Co_3O_4/CNTs-60, Co_3O_4/CNTs-80, Co_3O_4/CNTs-100, Co_3O_4/CNTs-120 and Co_3O_4/CNTs-140 corresponding to the above utrasonication time of CNTs. The nominal loading of Co in all catalysts was 15 wt%.

2.2. Characterizations of catalysts

The Co loading amount of samples was analyzed by J-A1100 inductively coupled plasma (ICP, Jarrell-Ash, U.S.A.). Transmission electron microscopy (TEM) measurements were carried out with JEOL-JEM-1010 transmission electron microscope at 100 kV. X-ray photoelectron spectroscopy (XPS) was carried out with an ESCALAB 250 electron spectrometer from Thermo of U.S.A. Raman spectra were employed at ambient temperature on a Renishaw inVia Raman Microscope with an argon-ion laser at an excitation wavelength of 514 nm. The temperature-programmed desorption of NH_3 (NH_3-TPD) was performed on a Micromeritics AutoChem 2920 II instrument. 200 mg of samples was preheated in He at 350 °C for 1 h, then cooled to 120 °C. NH_3–He (10 vol% NH_3) gas mixture was adsorbed at this temperature at the total flow rate of 40 ml/min until no signal variation of the gas was detected. Subsequently the sample was purged with He (40 ml/min) until no reactant was detected in the outlet, and then ramped to 630 °C at a linear heating rate of 8 °C/min in He (40 ml/min). Temperature-programmed reduction of hydrogen (H_2-TPR) was performed using a flow system equipped with a TCD detector. Typically, 50 mg of the samples was degassed at 100 °C for 1 h with argon gas flow, then cooled to 30 °C, and the gas flow was shifted to a mixture of 5 vol.% H_2 in Ar. The temperature was raised from 30 to 550 °C with a heating temperature rate of 10 °C/min. The water produced during reduction was trapped in a 5A molecular sieve column.

2.3. Catalytic reaction tests

The catalytic combustion of toluene was performed in a quartz U-type tube microreactor under atmospheric pressure. In the catalytic process, 200 mg of catalyst was placed in the reactor and then suffered thermal treatment at 400 °C for 3 h in N_2. When the temperature of the reactor decreased to 180 °C, the reactant gas of 850 ppm toluene in O_2/He mixture (20/80%) was fed into the reactor with the flow rate of 60 mL/min. The reactants and products were analyzed by an online gas chromatograph with a thermal conductivity and a flame ionization detector. Porapak Q column was used to detect for CO_2 and hydrocarbons and Molecular Sieve 5A for CO, O_2 and N_2. During the toluene oxidation, CO_2 and H_2O was almost the only reaction product observed. Only trace of CO was also observed at low conversions.

3. Results and discussion

3.1. Composition and morphology of the catalysts

The Co loadings detected by ICP were about 14.95, 14.93, 14.89, 14.87 and 14.91 wt% for Co_3O_4/CNTs-60, Co_3O_4/CNTs-80, Co_3O_4/CNTs-100, Co_3O_4/CNTs-120 and Co_3O_4/CNTs-140, respectively (Table 1). TEM images and the corresponding size distributions of overall particles reveal the morphology of Co_3O_4/CNT catalysts. It can be seen that CNTs with tubular structure have the diameters of 10–20 nm (Fig. 1a), and Co_3O_4 NPs were homogeneously dispersed on the surface of CNTs (Fig. 1b–f). Crystallite size distribution of Co_3O_4 is around 3–10 nm with a similar average size of 5–6.5 nm for each Co_3O_4/CNT catalyst (S1 of Supplementary Materials). XPS analysis was used to confirm the surface composition of the catalysts. Fig. 2A shows the Co 2p scan spectrum for each Co_3O_4/CNT sample. All the Co 2p spectra present two main peaks located at 780.9 and 796.1 eV, corresponding to Co $2p_{3/2}$ and Co $2p_{1/2}$, which indicates the formation of Co_3O_4 on CNTs [27]. The Co $2p_{3/2}$ signal of each catalyst could be deconvoluted to two components at 779.8 and 782.1 eV, ascribable to Co(III) and Co(II) [32], respectively. Quantitative analyses indicate that the proportion of Co(III)/Co(II) is essentially similar for all the prepared samples, close to 2/1 (Table 1). And the O 1s XPS spectra (Fig. 2B) were decomposed into two components at 529.2 and 531.3 eV, corresponding to the surface lattice oxygen (O_{latt}) and the adsorbed oxygen (O_{ads}) species [32]. The quantitative result reveals that the molar ratio of O_{ads}/O_{latt} for Co_3O_4/CNTs-60, Co_3O_4/CNTs-80, Co_3O_4/CNTs-100, Co_3O_4/CNTs-120 and Co_3O_4/CNTs-140 is 3.57, 5.08, 5.80, 9.17 and 6.06, respectively. This means that the adsorbed O_2 density on the catalysts follows the order of Co_3O_4/CNTs-60 < Co_3O_4/CNTs-80 < Co_3O_4/CNTs-100 < Co_3O_4/CNTs-140 < Co_3O_4/CNTs-120.

Co_3O_4 species on CNTs were also confirmed by XRD (Fig. 3). One can see that the representative XRD curves for CNTs-120 and Co_3O_4/CNTs-120 both display the peaks at 2θ of 26.2° and 44.2° (marked with Δ) for the (0 0 2) and (1 0 0) diffractions of hexagonal graphite, indicating that the graphite structure of the CNT supports is not destroyed during the ultrasonic treatment and the catalyst preparation [33]. 2θ at 31.3°, 36.8°, 44.8°, 59.3° and 65.2° (marked with *) could be perfectly indexed to a pure cubic phase of Co_3O_4 spinel (JCPDS 78-1970) on CNTs. Therefore, the results of TEM, XPS and XRD confirm the formation of Co_3O_4 NPs homogeneously dispersed on the surface of CNTs.

Table 1

Samples	Co content detected by ICP (wt%)	BET ($m^2\ g^{-1}$)	Pore size (nm)	Molar ratio of Co^{3+}/Co^{2+} detected by XPS	H_2-TPR	
					Two step reduction temperatures (°C)	Consumption hydrogen amount ratio
Co_3O_4/CNTs-60	14.95	245.6	12.08	1.95	343/444	22.5%/77.5%
Co_3O_4/CNTs-80	14.93	247.3	12.02	1.98	315/414	21.1%/78.9%
Co_3O_4/CNTs-100	14.89	246.9	11.03	2.05	292/387	20.7%/79.3%
Co_3O_4/CNTs-120	14.87	245.5	11.07	2.08	249/353	20.1%/79.9%
Co_3O_4/CNTs-140	14.91	247.8	11.09	2.11	309/410	21.7%/78.3%

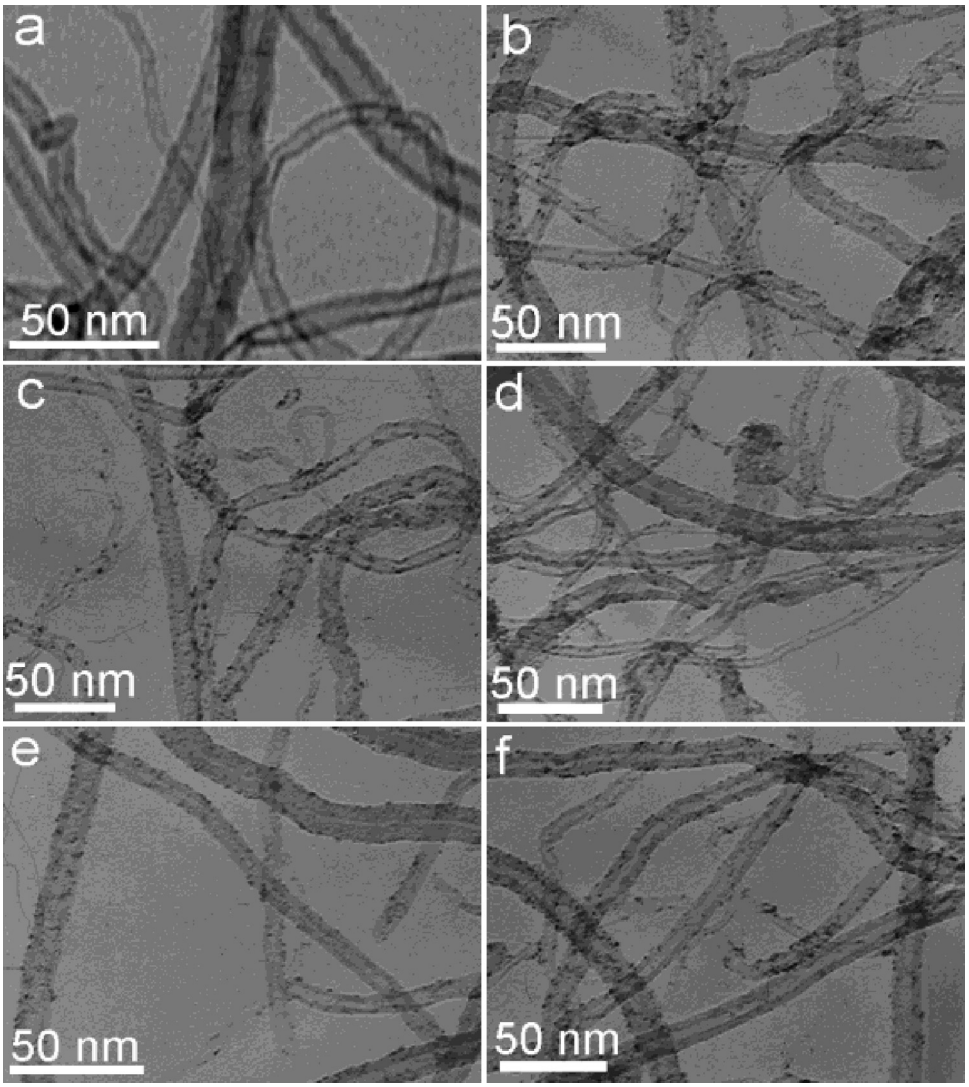

Fig. 1. TEM images of Co_3O_4/CNTs. (a) CNTs-120, (b) Co_3O_4/CNTs-60, (c) Co_3O_4/CNTs-80, (d) Co_3O_4/CNTs-100, (e) Co_3O_4/CNTs-120 and (f) Co_3O_4/CNTs-140.

3.2. Surface structure characterization of Co_3O_4/CNT catalysts

It is known that the catalytic performance of catalysts will be improved greatly by regulating the surface structures of the supports purposefully. Thus, it is necessary to investigate the surface structures of the CNT support and the corresponding Co_3O_4/CNT catalysts. It is known that the surface structures of the treated CNTs are composed of graphitize, oxygen-containing groups and defects. The defects including topological defects, incomplete bonding defects, rehybridization defects formed inevitably during the growth of CNTs or modification. Generally, the incomplete bonding structures are the mostly common defects which could be formed by destroying the conjugated π-bonds of the surface graphitize of CNTs, and the defects will be preferentially oxidized to —COOH.

Raman spectroscopy is often used to characterize the surface structures of CNTs. It can be seen that all the CNT samples present two main peaks at about 1342 and 1576 cm^{-1} (Fig. 4). The peak around 1342 cm^{-1} (D-band) is associated with the vibrations of carbon atoms in the disordered graphite structure, i.e., the defects. The peak at near 1576 cm^{-1} (G-band) corresponds to the E_{2g} mode of graphite. It is known that the ratio of the intensity of D-band to G-band (I_D/I_G) suggests the defect density in CNT samples and here the I_D/I_G is denoted as "*R*". As shown in Fig. 4, CNTs with ultrasonic treatment have different defect densities, and R values for CNTs are 0.85 (line a, CNTs-60), 0.95 (line b, CNTs-80), 1.00 (line c, CNTs-100), 1.09 (line d, CNTs-120) and 0.98 (line e, CNTs-140), respectively. It can be seen that the defect density of CNTs gradually increases and then decreases along with prolonging the ultrasonic time. It is reported that metal or metal oxides could be preferentially trapped by the surface defects of CNTs [34], and the formed metal-defect structures would facilitate the catalytic reaction [35]. Here, the location of the Co_3O_4 NPs on CNTs was investigated. Raman spectroscopy is also used for determining the deposition site of metal oxides on CNTs by comparing the defect density of CNTs before and after catalyst preparation [36]. In Fig. 4, it is found that the *R* is 0.85 for the pristine CNTs-60 and then decreases to 0.79 after Co_3O_4 loading. The defect densities in CNTs-80, CNTs-100, CNTs-120 and CNTs-140 show the same changes in this process, i.e., the *R* values decrease from 0.95 to 0.89, 1.00 to 0.94, 1.09 to 1.03 and 0.98 to 0.92, respectively. This indicates obviously that Co_3O_4 NPs should mainly anchor onto the defect structures of CNTs.

As another important surface structures of —COOH on CNTs, the amount of —COOH groups was determined with NH_3-TPD (Fig. 5) by measuring the desorption amount of NH_3 and the amount of the desorbed NH_3 was calculated by integrating the area of the desorption peak. (S2 of Supplementary Materials). The desorption amount of NH_3 on the pristine CNTs increased from 12 (CNTs-60)

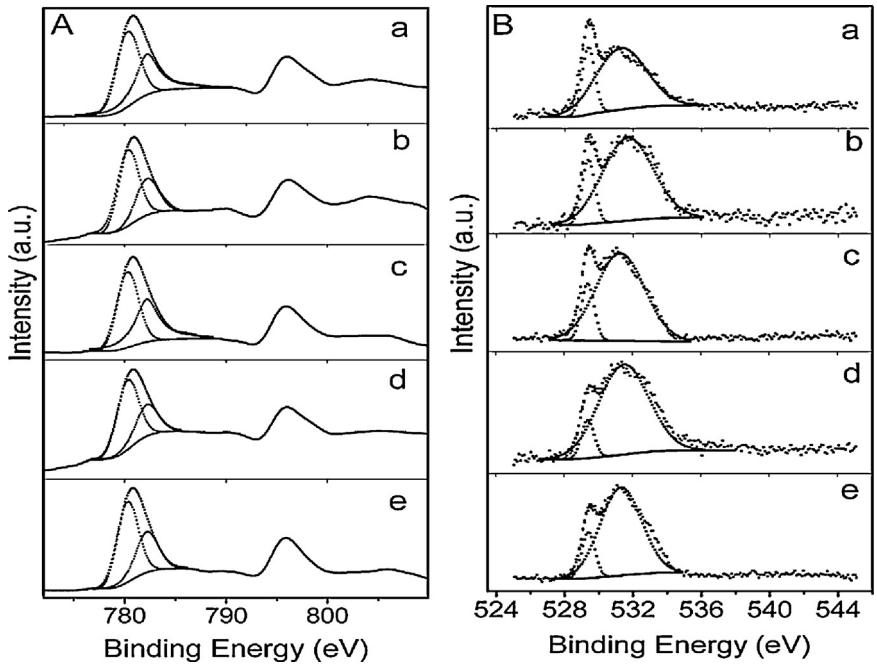

Fig. 2. (A) Co 2p XPS spectra and (B) O 1s XPS spectra for (a) Co_3O_4/CNTs-60, (b) Co_3O_4/CNTs-80, (c) Co_3O_4/CNTs-100, (d) Co_3O_4/CNTs-120 and (e) Co_3O_4/CNTs-140.

to 25 (CNTs-80), 59 (CNTs-100), 78 (CNTs-120) and 120 (CNTs-140) μmol/g (Fig. 5A), indicating an increase in the amount of —COOH groups on CNTs with prolonging the ultrasonication treatment time. After the formation of Co_3O_4 on CNTs, the desorption amount of NH_3 deceases to 3 (Co_3O_4/CNTs-60), 14 (Co_3O_4/CNTs-80), 50 (Co_3O_4/CNTs-100), 67 (Co_3O_4/CNTs-120) and 110 (Co_3O_4/CNTs-140) μmol/g, respectively (Fig. 5B). And the desorption amount of NH_3 on the pristine Co_3O_4 NPs prepared by hydrotherm method [37] is negligible, which is consistent with the study results of Zhao and Qiu et al. [38]. Further study indicates that the —COOH on CNTs plays an important role in the formation of Co_3O_4. In S3 of Supplementary Materials, it is learnt that the formation of Co_3O_4 on CNTs is attributed to the spontaneous redox reaction between CNTs and Co^{2+}, i.e., Co^{2+} is oxidized to Co^{3+} with the —COOH on CNTs as oxidant. Thus, part of —COOH on CNTs was consumed by the formation of Co_3O_4 on CNTs as reflected by the lowered desorption amount of NH_3 on Co_3O_4/CNTs than on the corresponding CNTs. Although the formed Co_3O_4 NPs could be preferentially trapped by the surface defects of CNTs, a few Co_3O_4 NPs would still anchor on the —COOH groups inevitably. Thus, the decrease of —COOH on CNTs should be attributed to the consumption of —COOH as oxidant and the anchor sites of a few Co_3O_4 NPs.

3.3. Reduction properties of Co_3O_4 supported on the surface of CNTs

The influence of the surface structures of CNTs on the reduction behavior of Co_3O_4 NPs was investigated by H_2-TPR (Fig. 6) since the redox behavior of the supported transition metal oxides is essential for the catalytic combustion reaction. The perfect graphitize

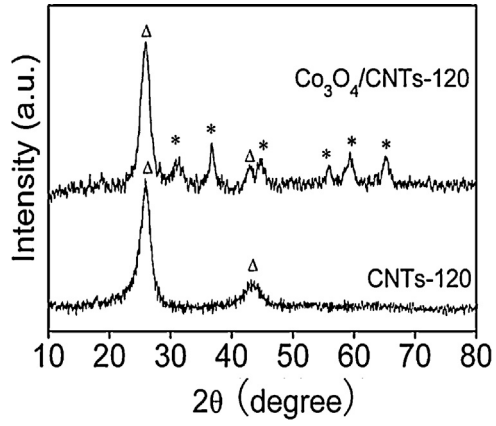

Fig. 3. XRD diffraction patterns of CNTs-120 and Co_3O_4/CNTs-120.

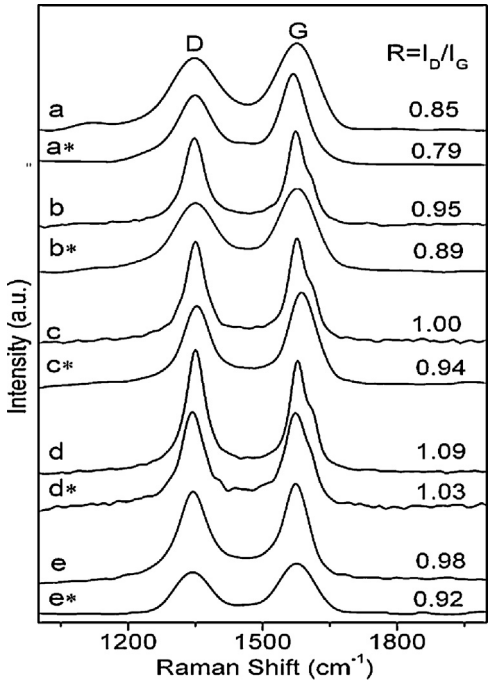

Fig. 4. Raman spectra of the CNTs and Co_3O_4/CNTs. (a) CNTs-60, (b) CNTs-80, (c) CNTs-100, (d) CNTs-120 and (e) CNTs-140; (a*) Co_3O_4/CNTs-60, (b*) Co_3O_4/CNTs-80, (c*) Co_3O_4/CNTs-100, (d*) Co_3O_4/CNTs-120 and (e*) Co_3O_4/CNTs-140.

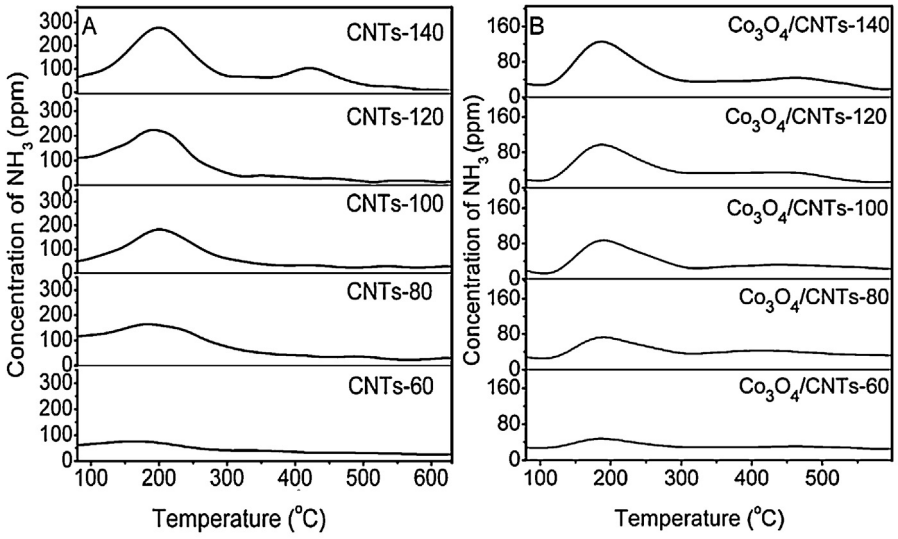

Fig. 5. NH_3-TPD profiles of (A) CNTs and (B) Co_3O_4/CNTs.

structures are considered as inert surface. By contrast, oxygen-containing groups (—COOH) and defect structures show interesting physical and chemical activities.

In Fig. 6 and Table 1, it is seen that there are two peaks in the range of 200–350 °C and 350–500 °C and the area ratio of the former peak to the latter one is about 1:3 for all samples, which indicates the two reduction processes of Co_3O_4 to CoO and CoO to Co. The two reduction peaks of Co_3O_4 NPs supported on CNTs-60, CNTs-80, CNTs-100, CNTs-120 and CNTs-140 are located at 343/444, 315/414, 292/387, 249/353 and 309/410 °C, respectively. Combined with the results of Figs. 3 and 4, the reduction temperatures of Co_3O_4 NPs decreased with increasing the defect density of CNTs. In order to further probe the influence of surface

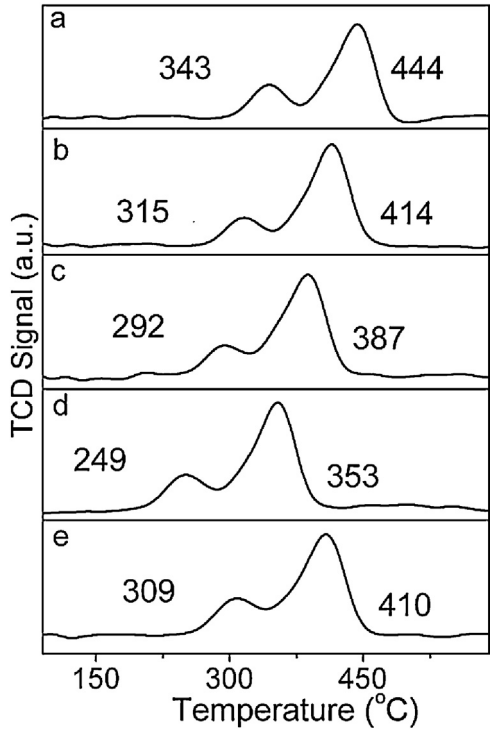

Fig. 6. H_2-TPR spectra of Co_3O_4/CNTs. (a) Co_3O_4/CNTs-60, (b) Co_3O_4/CNTs-80, (c) Co_3O_4/CNTs-100, (d) Co_3O_4/CNTs-120 and (e) Co_3O_4/CNTs-140.

structures of CNTs on the reduction of the supported Co_3O_4, Co_3O_4 NPs of 5–7 nm were deposited onto the highly graphitized CNTs and the CNTs with ultrasonic treatment for 90 min (denoted as Co_3O_4/CNTs-g and Co_3O_4/CNTs-90, respectively (S4 of Supplementary Materials). Similar to the reduction temperatures of 356/459 °C for pristine Co_3O_4 NPs, Co_3O_4 NPs supported on CNTs-g were reduced at 352/451 °C, indicating that CNTs-g can not greatly promote the reduction of Co_3O_4 due to the inertia of perfect graphitize structure. Moreover, CNTs-90 and CNTs-140 show the same defect density, while the amount of —COOH groups on Co_3O_4/CNTs-140 is much higher than that on Co_3O_4/CNTs-90. When Co_3O_4 supported on CNTs-90, the reduction temperatures are 298/391 °C. Whereas, Co_3O_4 supported on CNTs-140, the reduction temperatures increase to 309/410 °C. Furthermore, CNTs-100 and CNTs-120 have lower amount of —COOH, but higher defect density than CNTs-140. In the H_2-TPR (Fig. 6), the reduction temperatures of 292/387 °C (Co_3O_4/CNTs-100) and 249/353 °C (Co_3O_4/CNTs-120) for Co_3O_4 were obtained. Thus, it is seen that defects on CNTs can facilitate the reduction of Co_3O_4.

Study shows the defects of CNTs present electron acceptor-like states within graphitic materials and have a profound impact upon electronic transport properties [39]. Thus, the defects can facilitate electron transfer in the reduction process, which destabilizes the Co—O bonds and facilitates the reduction of Co_3O_4 in this study. The results mean that the defect of CNTs can enhance the ability of oxide catalysts to develop reduction/oxidation cycles, which is important in the combustion process and controls the catalytic behavior.

3.4. Catalytic performance

The thermal stability of the support material was analyzed by thermogravimetric analysis in air (S6 of Supplementary Materials). The weight loss is negligible in all cases below 400 °C, increasing particularly from 480 °C in the worst case. The result also indicates that the carboxylic groups on CNTs are stable and would not decarboxylated below 400 °C [40]. Therefore, the thermal stability of the catalyst guarantees the catalytic stability during the catalytic combustion of toluene operated below 400 °C here.

The catalytic activities of the Co_3O_4/CNT catalysts for the catalytic combustion of toluene were investigated in detail, and the catalytic results were shown in Fig. 7. The curves were used to describe the activity of Co_3O_4/CNT catalysts for the catalytic combustion of toluene, and only CO_2, H_2O, trace of CO and residual

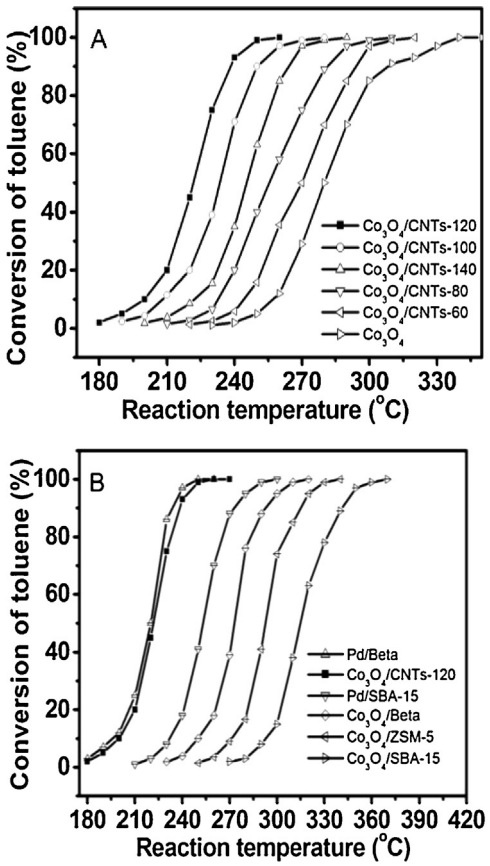

Fig. 7. (A) The conversion of toluene vs. temperature catalyzed by Co_3O_4/CNTs with different defect densities and the pristine Co_3O_4 NPs; (B) the catalytic combustion conversion of toluene vs. temperature catalyzed by Co_3O_4/CNTs-120, Pd and Co_3O_4 supported on zeolites.

toluene can be detected in the effluent regardless the catalysts used. The catalytic reaction on the pristine Co_3O_4 NPs starts at 231 °C and completes at 338 °C (Fig. 7A). When the Co_3O_4 NPs were supported on CNTs, the completed reaction temperature on Co_3O_4/CNT catalysts decreased significantly to 308 °C (Co_3O_4/CNTs-80), 272 °C (Co_3O_4/CNTs-100) and even to 257 °C (Co_3O_4/CNTs-120), then to 289 °C (Co_3O_4/CNTs-140). Although the particle size has been reported to affect the catalytic reaction, TEM characterization shows that the Co_3O_4 NPs supported on all CNTs are very similar in size (S1 of Supplementary Materials). Therefore, the particle size effect is probably not a crucial cause of the notably modified catalytic activity of Co_3O_4/CNTs compared with Co_3O_4 NPs observed in the above catalytic process. To understand the factors that determined the enhanced catalytic activity of Co_3O_4/CNTs, the mechanism of VOC oxidation reaction should be presented. In catalytic oxidation reaction, the catalytic behavior can be represented by a simple oxidation–reduction mechanism [41]:

$$\text{VOCs} + \text{oxidized catalyst} \rightarrow \text{reduced catalyst} + \text{oxidized product} \quad (1)$$

$$\text{Reduced catalyst} + O_2 \rightarrow \text{oxidized catalyst} \quad (2)$$

It is seen that two important factors directly determines the catalytic behavior, i.e., the reduction/oxidation behavior of the catalysts and the adsorbed O_2 density on the catalysts. Combined with the presented results here, it is interestingly found that increasing the defect density of CNT support could give rise to an increasing adsorbed O_2 density on the catalysts (Fig. 2B) and a decreasing reduction temperature of Co_3O_4 NPs (Fig. 6), which were both beneficial to enhance the catalytic activity of Co_3O_4/CNT catalysts (Fig. 7).

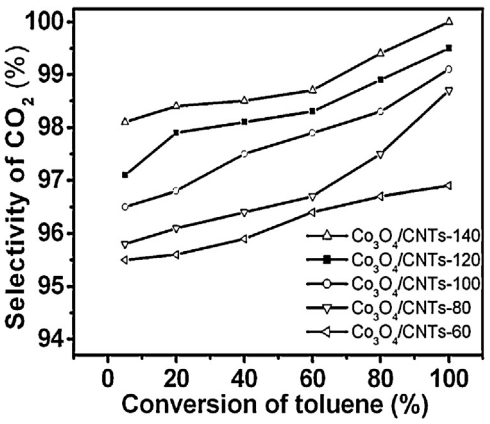

Fig. 8. The selectivity of CO_2 vs. the conversion of toluene catalyzed by Co_3O_4/CNTs with different —COOH amount.

Compared with Co_3O_4 supported on zeolites, Co_3O_4/CNTs-120 shows the superior catalytic activity (Fig. 7B), reflected by the order of the completed conversion temperature at Co_3O_4/CNTs-120 (257 °C) < Co_3O_4/Beta (317 °C) < Co_3O_4/ZSM-5 (335 °C) < Co_3O_4/SBA-15 (363 °C). Furthermore, Co_3O_4/CNTs-120 presents the higher catalytic performance than Pd/SBA-15 catalysts (299 °C). Compared with Pd/Beta catalyst (254 °C), Co_3O_4/CNTs-120 (257 °C) shows the similar catalytic activity. Moreover, the catalytic activity of Co_3O_4/CNTs-120 is better than that of the reported Au/CeO_2 [42], 3DOM-Co_3O_4, Co_3O_4 bulk [43], 9.5MnO_2/HCLT, 9.5Co_3O_4/HCLT [44], Pd/Co_3AlO (IMP), Pd/Co_3AlO (WIE) [45], and Au/Co_3O_4 [46]. Although inferior to that of Rod-like

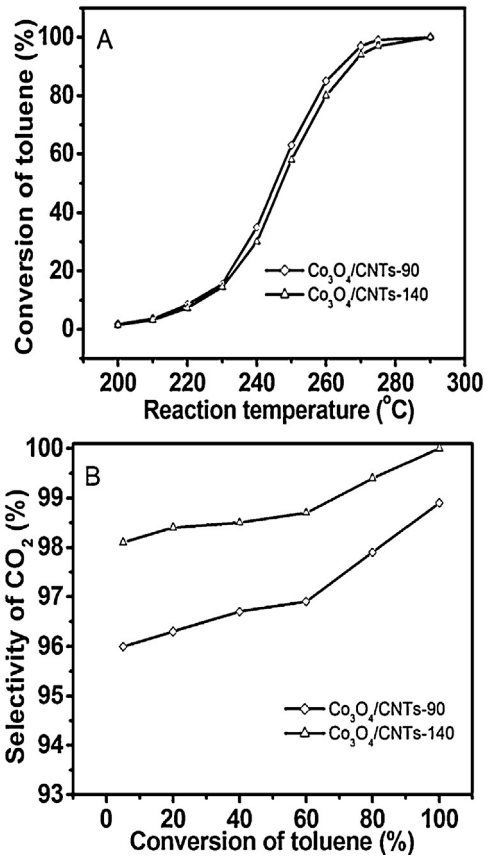

Fig. 9. (A) The catalytic conversion of toluene vs. temperature catalyzed by Co_3O_4/CNTs with different —COOH amount; (B) the corresponding selectivity of CO_2 in the catalytic reaction.

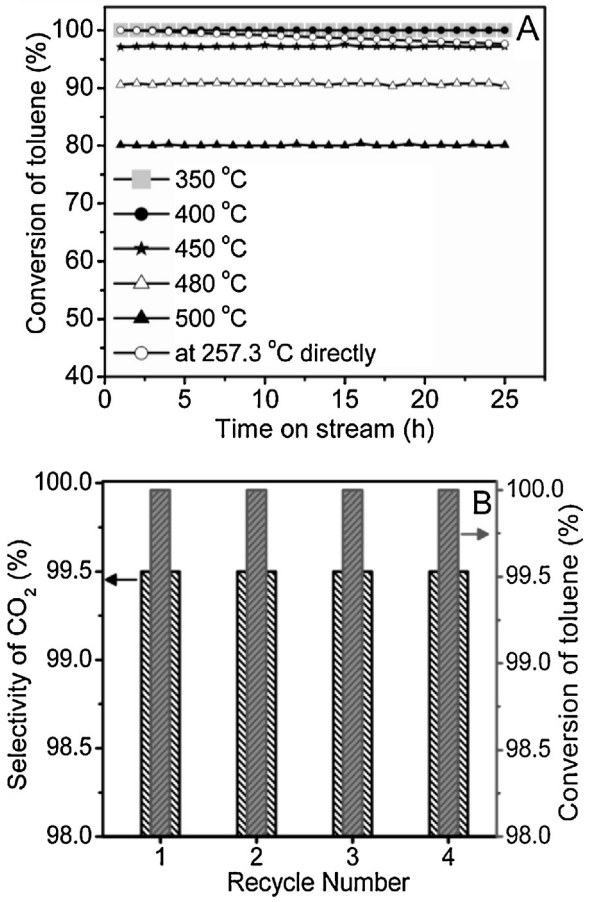

Fig. 10. (A) Time-on-stream behaviors of the catalytic combustion for toluene on Co_3O_4/CNTs-120 catalyst at 257 °C before (○) and after increasing the reaction temperature up to 350 (■), 400 (●), 450 (⋆), 480 (△) and 500 (▲) °C. (B) Repeated uses of Co_3O_4/CNTs-120 catalyst for the catalytic combustion of toluene.

MnO_2 [47], Pt-OMS-2 [7], $LaMnO_3$-PP-2 [18] and ordered cobalt oxides [25], the catalytic performance of the supported Co_3O_4 on CNTs could be further enhanced by increasing the defect density of CNTs facilely.

Besides the completed conversion temperature of toluene, the selectivity to CO_2 was also investigated. From Fig. 8, it can be seen that the CO_2 selectivity on the Co_3O_4/CNTs are 96.9% (Co_3O_4/CNTs-60), 98.7% (Co_3O_4/CNTs-80), 99.1% (Co_3O_4/CNTs-100), 99.5% (Co_3O_4/CNTs-120), and even reach 100% on Co_3O_4/CNTs-140. The results showed that the CO_2 selectivity in the catalytic combustion of toluene with the Co_3O_4/CNTs as catalysts increased with increasing the amount of —COOH on CNTs, indicating that the —COOH groups could promote the CO_2 selectivity. In order to further confirm the —COOH effect on the CO_2 selectivity in the catalysis, Co_3O_4/CNTs-90 was studied (Fig. 9). From the catalytic results, we can see that the complete reaction temperature (280 °C) for Co_3O_4/CNTs-90 is lower than that of Co_3O_4/CNTs-140 (289 °C), but the CO_2 selectivity for Co_3O_4/CNTs-140 is higher than that of Co_3O_4/CNTs-90. The results indicate that the —COOH structure of CNTs can enhance the CO_2 selectivity.

Moreover, the stability of Co_3O_4/CNTs was investigated in the catalytic combustion of toluene, and Co_3O_4/CNTs-120 as the representative was tested at 257 °C directly or after increasing reaction temperature to 350, 400, 450, 480 and 500 °C, respectively (Fig. 10A). The result indicates that the conversion of toluene in the catalytic combustion on Co_3O_4/CNTs-120 was maintained at ~98% after the reaction running for over 25 h (○ line). And the catalytic stability tested after increasing the reaction temperature up to 350 °C (■ line) or 400 °C (● line) presents perfect 100% conversion of toluene at 257 °C. After enhancing the reaction temperature to 450 °C (⋆ line), 480 °C (△ line) or 500 °C (▲ line), the conversion of toluene on Co_3O_4/CNTs-120 decreases from ~97% to 91% or 80% respectively during the 25 h stability tests, which is mainly arised from the distroyed structure of CNTs after 450 °C. The reuse of catalyst was also performed and the result for the four recycles of Co_3O_4/CNTs-120 is shown in Fig. 10B. Selectivity of CO_2 and conversion of toluene kept at perfect 99.5% and 100%, respectively. Thus, we can see that Co_3O_4/CNT catalyst not only provides high reactivity, but also presents good stability, indicating Co_3O_4/CNT catalyst is a good candidate for the catalytic combustion of toluene.

4. Conclusion

The above results reveal that the surface structures of CNTs does affect the catalytic performance of Co_3O_4 catalysts in the catalytic combustion of toluene. Study results showed that the surface defects of CNTs facilitated the catalytic combustion conversion of toluene, which was attributed to (i) the ability of Co_3O_4 to develop reduction/oxidation cycles was enhanced by the defects, (ii) the O_{ads}/O_{latt} molar ratio promoted by the defects. Moreover, the —COOH groups on CNTs could promote the selectivity to CO_2 in the catalytic combustion reaction. Thus, the conversion of toluene was completed at 257 °C, and the corresponding selectivity to CO_2 was about 100% with using Co_3O_4/CNTs as catalyst. Furthermore, compared with Pd/Beta and Pd/SBA-15 catalysts, Co_3O_4/CNTs showed a similar or even better catalytic performance. These results indicate that transition metal oxides supported on CNTs have a great potential application in the catalytic combustion of VOCs by tuning the surface structures of CNTs.

Acknowledgments

We gratefully acknowledge the support from the National Natural Science Foundation of China (21103019), the Foundation of Key Laboratory of Radioactive Geology and Exploration Technology Fundamental Science for National Defense (REGT1214 and 2010RGET15) and the Start-up Fund of the East China Institute of Technology (DHBK1005 and DHBK1009).

Appendix A. Supplementary data

Supplementary data associated with this article can be found, in the online version, at http://dx.doi.org/10.1016/j.apcatb.2013.03.040.

References

[1] K. Everaert, J. Baeyens, Journal of Hazardous Materials 109 (2004) 113–139.
[2] F. Diehl, J. Barbier Jr., D. Duprez, I. Guibard, G. Mabilon, Applied Catalysis B: Environmental 95 (2010) 217–227.
[3] C. He, P. Li, H.L. Wang, J. Cheng, X.Y. Zhang, Y.F. Wang, Z.P. Hao, Journal of Hazardous Materials 181 (2010) 996–1003.
[4] N. Kamiuchi, T. Mitsui, N. Yamaguchi, H. Muroyama, T. Matsui, R. Kikuchi, K. Eguchi, Catalysis Today 157 (2010) 415–419.
[5] L.F. Liotta, Applied Catalysis B: Environmental 100 (2010) 403–412.
[6] C. He, J.J. Li, P. Li, J. Cheng, Z.P. Hao, Z.P. Xu, Applied Catalysis B: Environmental 96 (2010) 466–475.
[7] O. Sanz, J.J. Delgado, P. Navarro, G. Arzamendi, L.M. Gandia, M. Montes, Applied Catalysis B: Environmental 110 (2011) 231–237.
[8] A. Aznarez, F.C.C. Assis, A. Gil, S.A. Korili, Catalysis Today 176 (2011) 328–330.
[9] B. Solsona, M. Perez-Cabero, I. Vazquez, A. Dejoz, T. Garcia, J. Alvarez-Rodriguez, J. El-Haskouri, D. Beltran, P. Amoros, Chemical Engineering Journal 187 (2012) 391–400.
[10] C. He, J.R. Li, X.Y. Zhang, L.Q. Yin, J.S. Chen, S.K. Gao, Chemical Engineering Journal 180 (2012) 46–56.
[11] C. He, F.W. Zhang, L. Yue, X.S. Shang, J.S. Chen, Z.P. Hao, Applied Catalysis B: Environmental 111/112 (2012) 46–57.
[12] M.N. Taylor, W. Zhou, T. Garcia, B. Solsona, A.F. Carley, C.J. Kiely, S.H. Taylor, Journal of Catalysis 285 (2012) 103–114.

[13] M. Hosseini, T. Barakat, R. Cousin, A. Aboukais, B.L. Su, G.D. Weireld, S. Siffert, Applied Catalysis B: Environmental 111/112 (2012) 218–224.
[14] A. Perez, J.F. Lamonier, J.M. Giraudon, R. Molina, S. Moreno, Catalysis Today 176 (2011) 286–291.
[15] A. Perez, M. Montes, R. Molina, S. Moreno, Applied Catalysis A: General 408 (2011) 96–104.
[16] D.A. Aguilera, A. Perez, R. Molina, S. Moreno, Applied Catalysis B: Environmental 104 (2011) 144–150.
[17] Y.X. Liu, H.X. Dai, Y.C. Du, J.G. Deng, L. Zhang, Z.X. Zhao, Applied Catalysis B: Environmental 119/120 (2012) 20–31.
[18] Y.X. Liu, H.X. Dai, Y.C. Du, J.G. Deng, L. Zhang, Z.X. Zhao, C.T. Au, Journal of Catalysis 287 (2012) 149–160.
[19] Z.X. Zhao, H.X. Dai, J.G. Deng, Y.C. Du, Y.X. Liu, L. Zhang, Microporous and Mesoporous Materials 163 (2012) 131–139.
[20] F.J. Shi, F. Wang, H.X. Dai, J.X. Dai, J.G. Deng, Y.X. Liu, G.M. Bai, K.M. Ji, C.T. Au, Applied Catalysis A: General 433/434 (2012) 206–213.
[21] Y.C. Du, Q. Meng, J.S. Wang, J. Yan, H.G. Fan, Y.X. Liu, H.X. Dai, Microporous and Mesoporous Materials 162 (2012) 199–206.
[22] K.M. Ji, H.X. Dai, J.G. Deng, L.Y. Song, B.Z. Gao, Y. Wang, X.W. Li, Applied Catalysis B: Environmental 129 (2013) 539–548.
[23] W. Zhao, J. Cheng, L.N. Wang, J.L. Chu, J.K. Qu, Y.H. Liu, S.H. Li, H. Zhang, J.C. Wang, Z.P. Hao, T. Qi, Applied Catalysis B: Environ. 127 (2012) 246–254.
[24] B.D. Rivas, R. Lopez-Fonseca, C. Jimenez-Gonzalez, J.I. Gutierrez-Ortiz, Chemical Engineering Journal 184 (2012) 184–192.
[25] T. Garcia, S. Agouram, J.F. Sánchez-Royo, R. Murillo, A.M. Mastral, A. Aranda, I. Vázqueze, A. Dejoze, B. Solsona, Applied Catalysis A: General 386 (2010) 16–27.
[26] B.D. Rivas, R. Lopez-Fonseca, C. Jomenez-Gonzalez, J.I. Gutierrez-Ortiz, Journal of Catalysis 281 (2011) 88–97.
[27] Q.Y. Yan, X.Y. Li, Q.D. Zhao, G.H. Chen, Journal of Hazardous Materials 209-210 (2012) 386–391.
[28] D. Tasis, N. Tagmatarchis, A. Bianco, M. Prato, Chemical Reviews 106 (2006) 1105–1136.
[29] S.Q. Song, H.X. Yang, R.C. Rao, H.D. Liu, A.M. Zhang, Catalysis Communications 11 (2010) 783–787.
[30] S.X. Yang, X. Li, W.P. Zhu, J.B. Wang, C. Descorme, Carbon 46 (2008) 445–452.
[31] S.Q. Song, S.J. Jiang, Applied Catalysis B: Environmental 117/118 (2012) 346–350.
[32] Y.S. Xia, H.X. Dai, H.Y. Jiang, L. Zhang, Catalysis Communications 11 (2010) 1171–1175.
[33] T. Belin, F. Epron, Materials Science and Engineering B 119 (2005) 105–118.
[34] J.A. Rodriguez-Manzo, O. Cretu, F. Banhart, ACS Nano 4 (2010) 3422–3428.
[35] S.Q. Song, S.J. Jiang, H.X. Yang, R.C. Rao, A.M. Zhang, Applied Catalysis A: General 401 (2011) 215–219.
[36] S.J. Kim, Y.J. Park, E.J. Ra, K.K. Kim, K.H. An, Y.H. Lee, J.Y. Choi, C.H. Park, S.K. Doo, M.H. Park, C.W. Yang, Applied Physics Letters 90 (2007) 023114.
[37] Y.M. Dong, K. He, L. Yin, A.M. Zhang, Nanotechnology 18 (2007) 435602.
[38] B. Meng, Z.B. Zhao, X.Z. Wang, J.J. Liang, J.S. Qiu, Applied Catalysis B: Environmental 129 (2013) 491–500.
[39] S.Q. Song, H.X. Yang, R.C. Rao, H.D. Liu, A.M. Zhang, Applied Catalysis A: General 375 (2010) 265–271.
[40] V. Datsyuk, M. Kalyva, K. Papagelis, J. Parthenios, D. Tasis, A. Siokou, I. Kallitsis, C. Galiotis, Carbon 46 (2008) 833–840.
[41] M.A. Alvarez-Merino, M.F. Ribeiro, J.M. Silva, F. Carrasco-Marin, F.J. Maldonado-Hodar, Environmental Science and Technology 38 (2004) 4664–4670.
[42] M. Ousmane, L.F. Liotta, G. Di Carlo, G. Pantaleo, A.M. Venezia, G. Deganello, L. Retailleau, A. Boreave, A. Giroir-Fendler, Applied Catalysis B: Environmental 101 (2011) 629–637.
[43] K.M. Ji, H.X. Dai, J.G. Deng, X.W. Li, Y. Wang, B.Z. Gao, G.M. Bai, C.T. Au, Applied Catalysis A: General 447/448 (2012) 41–48.
[44] G.S.P. Spylu, Z. Ozcelik, L. Boz, Chemical Engineering Journal 162 (2010) 380–387.
[45] P. Li, C. He, J. Cheng, C.Y. Ma, B.J. Dou, Z.P. Hao, Applied Catalysis B: Environmental 101 (2011) 570–579.
[46] H.J. Wu, L.D. Wang, Z.Y. Shen, J.H. Zhao, Journal of Molecular Catalysis A: Chemical 351 (2011) 188–195.
[47] F. Wang, H.X. Dai, J.G. Deng, G.M. Bai, K.M. Ji, Y.X. Liu, Environmental Science and Technology 46 (2012) 4034–4041.